JOURNAL OF AIRCRAFT
Vol. 47, No. 2, March–April 2010

Crosswind Effects on Engine Inlets: The Inlet Vortex

Luís Gustavo Trapp*
Embraer, 12227-901 São José dos Campos, Brazil
and
Roberto da Motta Girardi†
Instituto Tecnológico de Aeronáutica, 12228-900 São José dos Campos, Brazil

DOI: 10.2514/1.45743

The effects of the inlet vortex on engines operating near the ground have been studied for more than 50 years, but the phenomenon is not yet completely understood. In this work a review of the past research is conducted, together with the existing patents of systems that protect the engine from vortices. Computational fluid dynamics is then used, on a DLR-F6 modified nacelle, to allow a more detailed look into the inlet-vortex phenomenon, its origin and the effect it has on ground pressures. It is also shown that the trailing vortex, which coexists with the inlet vortex, originates on the nacelle surface and is ingested by the inlet. Three different inlet-vortex intensity regimes are defined and new correlations are proposed to evaluate the existence of inlet vortices.

Nomenclature

A	=	area
CR	=	contraction ratio, A_h/A_i
D	=	diameter
DR	=	diffusion ratio, A_f/A_i
H	=	distance from the engine axis to the ground
L	=	length
L_i	=	interference length
M	=	Mach number
MFR	=	mass flow ratio, $U_i/U_0 = A_0/A_i$
U	=	time-averaged velocity
SDR	=	stream-tube diameter ratio, $D_0/2H$
W	=	engine mass flow rate
Z	=	distance from the inlet lip to the ground

Subscripts

e	=	engine inlet
ex	=	exhaust
f	=	fan station
h	=	inlet highlight station
i	=	inlet throat station
m	=	maximum
0	=	freestream

I. Introduction

WIND is one of the most adverse environmental factors that influence aircraft ground handling and, particularly, engine operation. A wind misaligned with the aircraft can impact all aspects of its ground operation: namely, start, taxiing, takeoff, and landing. However, it is during takeoff that the wind has the greatest effect on the engines, especially when the aircraft is static at the runway threshold, at high power, just before brake release and the beginning of the takeoff roll. This high-power static engine is affected by crosswind through three different aspects: fuselage vortex shedding, inlet separation, and ground vortex. All these phenomena produce a nonuniform airflow that is ingested by the inlet, affecting the engine operation and maybe even affecting its physical integrity. This nonuniform flow ingested by the engine is generally referred to as inlet distortion or distortion, which can be assessed through standard procedures (e.g., [1]).

The inlet-vortex forms between the engine inlet and the ground at very low aircraft speeds and is created by the interaction between the inlet flow and the crosswind, which is able to suck considerably large objects into the engine. It can also affect engine operability when it is ingested by the engine core.

The goal of this work is to study the nacelle inlet under crosswinds conditions using computational fluid dynamics (CFD) tools, taking a more detailed look into the inlet-vortex phenomenon, its origin, and the effect it has on ground pressures.

An engine ingests air to operate and this volume of air can defined by a stream tube (see Fig. 1), which has a cross section A_0 and freestream speed V_0. As the air approaches the engine, this stream tube is accelerated into the inlet, reaching a speed V_i at the inlet throat of area A_i. If the engine is operating near the ground at high power, the engine stream tube will encompass part of the ground surface, where it will induce flow. This induced flow on the ground will, in turn, also encompass the ground debris, eventually sucking them into the engine and leading to engine damage (also called foreign-object damage). Even if the ingested particles are small and do not damage the engine instantaneously, they can increase blade erosion or lead to dust deposits inside the engine, decreasing its life.

The sole existence of induced velocities on the ground does not mean that there is the risk of foreign-object ingestion because these velocities alone are not high enough to lift the debris. The main cause of foreign-objects intake by the engine is the inlet vortex: a strong vortex that builds up between the ground and the engine. The inlet vortex is able to lift particles from the ground, which are much larger than the ones carried by the average inlet flow because of the vortex higher flow speed and lower pressure. Klein [2] mentions that the average suction force on the ground of an inlet flow with no vortex is less than 1 lb. On the other hand, an inlet flow with a vortex produces a force of about 40 lb. Figures 2–4 show inlet vortices in different applications. Although the vortex is not usually visible, under humid ambient conditions the vortex core can condensate, making it visible. Also, the vortex can be seen when it goes through water standing on the ground. The figures show that inlet vortices exist on high wing configurations and even on propeller driven aircraft.

Each year, engine foreign-object damage cost billions of dollars and is a great source of concern to airlines, airports, and aircraft manufacturers. To avoid these costs and damages, the intake of foreign objects by inlet vortices has been an object of research for more than 50 years. The initial attempts to study the inlet vortex used

Received 31 May 2009; revision received 22 September 2009; accepted for publication 25 September 2009.

*Propulsion Systems Engineer, Center of Competence, Avenida Faria Lima 2170.

†Professor, Aeronautical and Mechanical Engineering Department, Praça Marechal Eduardo Gomes 50.

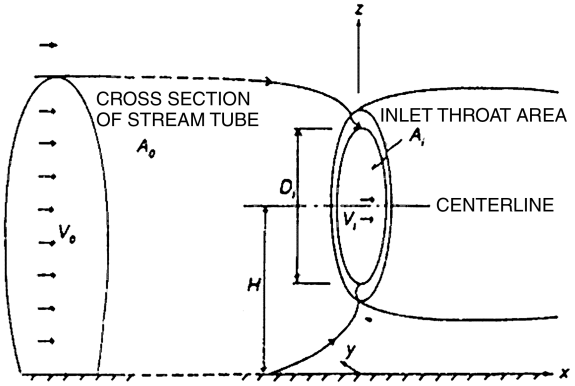

Fig. 1 Engine stream tube reaching the ground [13].

Fig. 2 Ground vortex at test stand [9].

engines on test stands and soon afterwards scaled model inlets were tested in wind tunnels. In the 1970s, computers and panel method codes started to be used to evaluate the phenomenon, while in the last decade CFD has been used to further understand the inlet vortex. In 1955, Rodert and Garrett [3] were probably the first authors to publish about the jet engine inlet vortex in open literature. They performed experiments on an engine capable of producing 5000 lb of thrust, installed on an old high-wing aircraft, testing the engine with different power settings and distances to the ground. The engine inlet was modified and a protective grid was added to the inlet pipe so that foreign objects would not get into the engine. To collect data in their

Fig. 3 Ground vortex on an YC-14 aircraft [30].

Fig. 4 Ground vortex on a C-130 aircraft propeller [30].

experiment, they tried different visualization techniques, including placing wool tufts, water, and powdered talc on the ground and, with the grid protection installed on the engine inlet, even actual stones. Static pressures on the ground at fixed locations were measured (the lowest one being approximately 12% lower than ambient). They also found that objects sitting on runway cracks are more easily sucked than the ones exposed on a smooth surface and that the vortex existence was a function of engine power, distance to the ground, wind speed, and direction.

Klein [2] also performed some experiments and found that the intensification of both the vertical upward flow of air (or engine suction) and the circulatory flow present on the ambient increases the magnitude and power of the inlet vortex, therefore increasing its ability to project heavier objects upward and into the engine inlet.

Glenny and Pyestock [4] also investigated the ingestion of foreign objects due to inlet vortices but this time using a scaled model nacelle in a wind tunnel with the objective of determining the foreign-object ingestion thresholds. The authors analyzed the phenomenon using scale laws and dimensionless groups, like the inlet throat-to-wind velocity ratio U_i/U_0 and the ratio between engine axis height to the ground and inlet diameter (H/D_i, or nondimensional height). In their experiments, the inlet nondimensional height was varied between 0.9 and 1.8 and they imposed different external flow velocity gradients. Despite investigating different options for reducing the ingestion of debris, they were not able to find any definitive solution. They proposed a takeoff operational technique where the engine power was progressively increased as the aircraft speed increased, therefore keeping an engine inlet mass flow rate that reduced the inlet stream-tube contact with the ground (see Fig. 1). They also verified that the speed where the vortex ceased to exist (vortex clear-out speed or vortex blow-away speed) increased as the wind direction moved from head to tailwind. They found that the vortex strength was influenced by the wind spatial velocity gradient: when there was a uniform wind, the inlet vortex was barely noticed. Also, when there was no wind, the vortex did not appear, even if the inlet flow was increased to the point of choking.

The first author to propose the minimum requirements for an inlet vortex to exist was Klein [2] in 1959, conditioning that

1) A stagnation point must exist on the ground (or other fixed structure), where an omnidirectional air flow parallel to the surface converges in a manner similar to a sink.

2) There must be an updraft from the stagnation point to the inlet.

3) Ambient vorticity must be present in the flow.

Shin et al. [5] added that an inlet flow coming at an angle (side winds) would generate circulation around the inlet, making up for the requirement of ambient vorticity.

Klein [6] tested two inlets on top of each other (see Fig. 5 from De Siervi [7]), in a wind tunnel with a crossflow. He found that an inlet vortex would still form between the two inlets, showing that it is not necessary to have a ground boundary layer for the inlet vortex to exist and that is not vorticity generated on the ground surface that is responsible for the appearance of the vortex or is responsible for sustaining it.

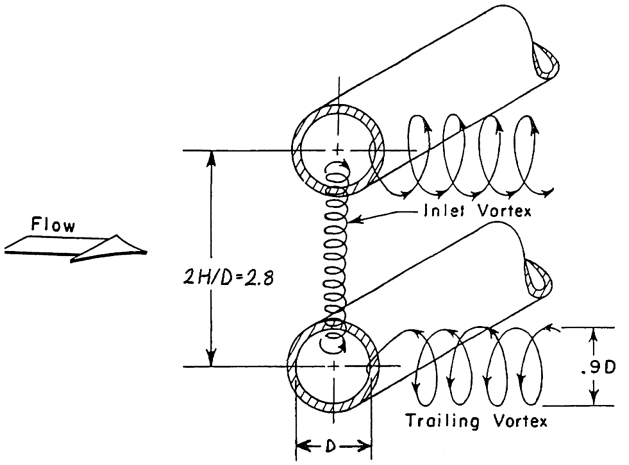

Fig. 5 Experiment with two inlets on top of each other in a crossflow [7].

De Siervi [7] studied inlet vortices using scaled nacelle models in a water tunnel and visualizing the flow using hydrogen bubbles. The tests involved subjecting the inlet to both irrotational and shear flows, the latter being used to evaluate the inlet vortex behavior under different flow vortices, including vorticity approaching the inlet with its direction opposite to that of a ground boundary layer. These flow profiles influenced the strength of the inlet vortex and the direction of the vortex rotation. During the experiments, the author showed that when the inlet axis was aligned with the flow, and the flow was rotational, there were two contrarotating vortices close to each other in the inlet face bottom. When the flow was irrotational and aligned with the inlet axis, there was no inlet vortex.

De Siervi [7] detected a previously unknown feature of the flow: besides the ground vortex, there was another vortex (the trailing vortex) that originated at the inlet and trailed downstream of it, as shown in Fig. 6. Both trailing and ground vortices had roughly the same circulation intensity but opposite directions. The cores of the vortices were also different: whereas the inlet vortex size was set by a balance between diffusion and convection, the trailing vortex size was dictated by the size of the separated region behind the inlet. Another vortex feature was that when the flow approached the inlet from the left with a boundary layer shear flow, the inlet vortex rotated clockwise (Fig. 6), whereas when the crossflow direction was the opposite, the vortex rotational direction was counterclockwise.

Observations made by De Siervi [7] and Liu et al. [8] described the vortex existence as a function of the inlet capture area. If the crossflow velocity is high or the inlet mass flow rate is low, the capture area does not reach the ground and there will be two counter-rotating trailing vortices (Fig. 7); if the mass flow is high or the wind speed low, there will be an inlet vortex attached to the ground and a trailing vortex downstream of the inlet (Fig. 8).

Liu et al. [8] also performed experiments in a wind tunnel, with an axisymmetrical nacelle model close to the ground measuring static pressures at different inlet axial and longitudinal locations. They also visualized the inlet flow using surface paint on Plexiglas® model and the vortex flow using smoke and tufts on the floor. They tested inlet

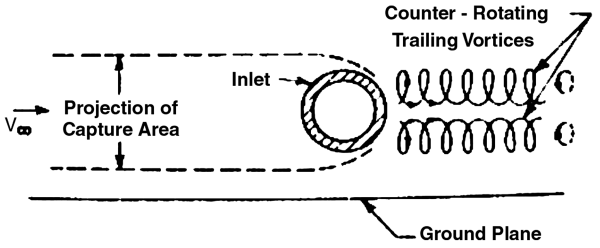

Fig. 7 Inlet capture area under a low mass flow ratio [8].

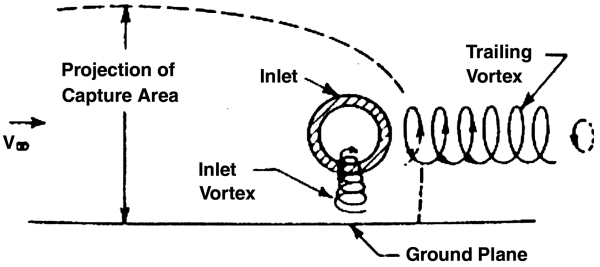

Fig. 8 Inlet capture area under a high mass flow ratio [8].

height ratios H/D of 1.0, 1.5, and 2.0, with mass flow ratios between 5 and 30 and determined the boundaries of the vortex/no vortex regimes to be located at

$$\frac{U_i D_i^2}{U_0 D_m^2} = 17.3\frac{H}{D_i} - 0.5 \tag{1}$$

where U_i is the inlet throat speed, U_0 is the freestream speed, D_i is the inlet throat diameter, D_m is the nacelle external diameter, and H is the height from the inlet axis to the ground.

Brix et al. [9] performed an extensive wind-tunnel test campaign on a scaled model nacelle (Fig. 2), measuring the inlet flow velocity distribution using rotating split-fiber probes for different crossflow angles and speeds. They discovered another vortex regime that does not require any ambient flow around the inlet.

Panel methods have been used since the 1970s to study the inlet vortex phenomenon and understand the engine behavior near the ground. Colehour and Farquhar [10] used sinks and vortices to understand the inlet vortex phenomenon and develop techniques to prevent its formation; they also performed some experiments and described methods for vortex suppression in stationary applications. Motycka et al. [11] tried to evaluate the distortion caused by the inlet vortex on the engine face and determine the location of the inlet vortex with varying wind direction and intensity. Their study aimed at determining the engine inlet flow to evaluate the susceptibility of the engine core to vortex ingestion because of its effects on engine operability. They showed (Fig. 9) that the vortex core location moves in the wind direction (being more prone to enter the engine core with tailwinds). The inlet-vortex diameter can be of the same order of magnitude of engine compressor blade, but it is small if compared to the fan blade. If the vortex is ingested by the engine core, the local

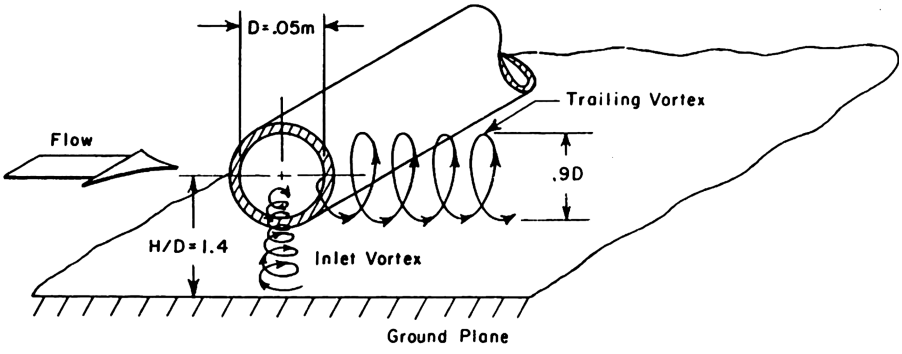

Fig. 6 Inlet vortices in a crossflow [7].

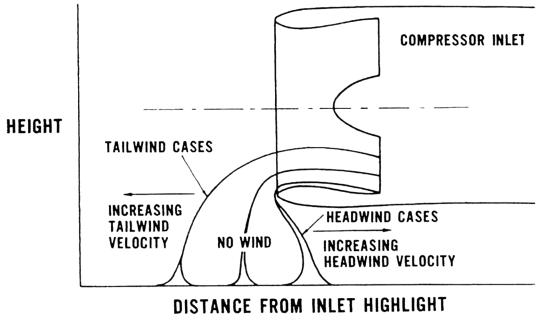

Fig. 9 Vortex position as a function of wind direction [11].

flow can be disrupted, leading to compressor blades stall and, as a consequence, to engine surge.

Viguier [12] also performed simulations of the inlet-vortex phenomenon using panel methods; however, the limitations of the method allowed only a qualitative analysis of the phenomenon. Nakayama and Jones [13] performed some calculations using a panel method code with compressibility correction. Even though their code would not be able to show an inlet vortex, they correlated the existence of inlet vortices to the existence of a stagnation line between the ground and the inlet. Because of the limited resources at the time, the authors could not perform a viscous analysis or use turbulent models, mainly because of the relative size of the inlet vortex core compared to the inlet, which would require grids beyond their computational capability. They suggested that inviscid analyses do not give reasonable results, with vortex clearance speeds being lower than experimental data. Nakayama and Jones [13] also proposed, based on their as well as other authors' experimental data, that the limit between the vortex and no vortex regimes is located at

$$\text{MFR} = \frac{U_i}{U_0} = 24\frac{H}{D_i} - 17 \tag{2}$$

More recently, CFD tools have also been applied to simulate the inlet vortex with relative success. Tourrette [14] used wind-tunnel experimental data of a nacelle in crossflow to validate a CFD code, finding reasonable agreement between the results. Secareanu et al. [15] also performed experiments and large eddy simulation with an isolated nacelle close to the ground. The experimental setup involved a nacelle simulated by a short pipe with suction on one side located at height ratio of unity, where the vortex flow was measured using particle image velocimetry (PIV). The experimental results showed agreement with the CFD only away from the vortex, both because the vortex frequency was too great for the PIV used and because the CFD analysis results were questionable due to the high Reynolds number.

Yadlin and Shmilovich [16] performed CFD analyses of inlet vortices on a Boeing C-17 cargo airplane with thrust reversers deployed. The analysis was performed using overset grids, preconditioning, and the shear stress transport (SST) turbulence model with different head and tailwind intensities. Figure 10 shows results of peak force suction on the ground as the wind changes from tail to head wind. The analyses were performed on two models of different complexity: isolated nacelles close to the ground and a model including aircraft wings and fuselage. Because of the complexity of the phenomenon, the authors performed only a qualitative analysis, being interested in establishing a procedure that would help them develop a protection system to minimize the existence of inlet vortices.

Rehby [17] performed CFD analysis of an isolated nacelle near the ground to study its major features, determining vortex characteristics and the effects on it of the nondimensional height, the inlet mass flow, and the freestream velocity. The hexahedral mesh contained over 1.3 million elements and steady-state analyses were performed using the k-ω SST turbulence model. Comparisons of the computational results with experiments performed at Cranfield University showed good similarities in terms of circulation, total pressure, and vortex locations, but the CFD results seemed to overestimate the real values.

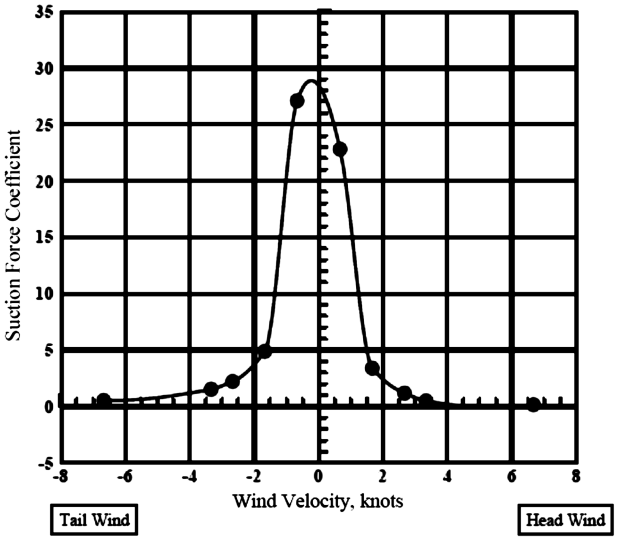

Fig. 10 Suction force on the ground as function of wind velocity [16].

II. Damage Protection Inventions

During the evolution of the jet engine, different systems were developed to avoid foreign-object ingestion: usually the outcome of research into inlet vortices. All these inventions tried to make the aircraft rely less, or not even rely at all, on airport runway cleaning because of its imperfect results and high operating costs. Some of the systems also tried to make possible the operation of jet engine aircraft on unpaved or gravel runways.

According to Johns [18], the first inlet-vortex prevention system to be put into commercial service was the blow-away jet used on the DC-8 aircraft in the late 1950s and early 1960s. Figure 11 shows from the blow-away patent from Klein [2]. This system uses a continuous flow bled from the engine, creating a single jet exhausted near the inlet lip and directed toward the vortex stagnation line. The jet impinging on the vortex stagnation line weakened the vortex, which tended to disappear.

The success of this system was hindered by the fact that the ground vortex position is influenced by different external factors, like the local wind intensity and direction, as well as the engine thrust setting, therefore sometimes it was not possible to impinge the vortex stagnation line when operating out of the design condition. Even worse was that along with impinging the vortex stagnation line, the jet flow also impinged the debris on the ground, projecting them up, sometimes getting them entrained into the inlet flow and provoking the exact damage it was intended to avoid.

Lee [19] proposed an inlet protection system for a vertical takeoff and landing aircraft with nacelles that turned vertically during takeoff and landing. The downward exhaust plume could lift debris up, which could eventually be ingested by the inlet from all directions; therefore, the protection system had to have an omnidirectional protection. It consisted of two features: the first being simply to close

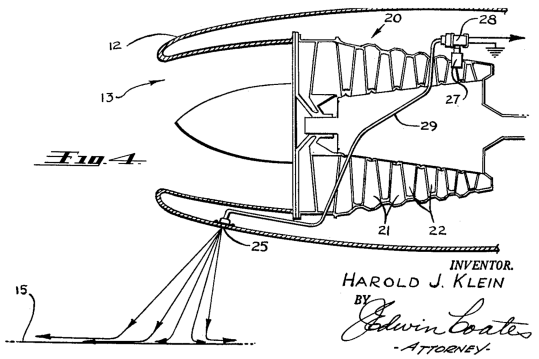

Fig. 11 Blow-away jet system for inlet-vortex avoidance, image from the patent of Klein [2].

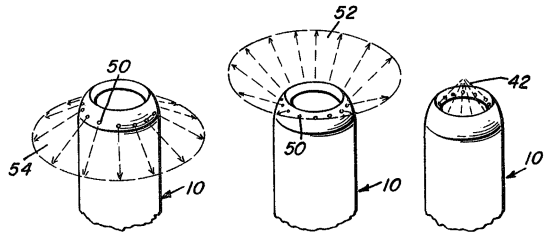

Fig. 12 Protection system where bleed flow used to shield the surrounding of the inlet from debris [19].

the inlet completely during ground operation using thin blades. To allow the engine to continue working, liquid air was to be fed into the engine through a dedicated piping system. The second feature involved creating a flow barrier that prevented foreign particles from entering the inlet. This additional system was necessary to avoid matter accumulation on the closed inlet and its ingestion as soon as the system was opened after takeoff. Drawings of different ways of accomplishing this secondary feature are shown on Fig. 12 (with engine air bled and exhausted at different locations on the inlet lip). Because the inlet plane is almost horizontal when operating near the ground, the flow barrier does not impinge the ground, therefore avoiding lifting debris opposed to Klein's system [2]. However, this system proposed by Lee was not practical, starting with the aircraft lifting system that was completely based on engine thrust and on a nacelle that could turn and point downwards. Another drawback was the heavy air feeding system needed to run the engine during the takeoffs, when the inlet was supposed to be completely closed.

A different approach to protect an underwing podded engine inlet was proposed by Cox and William [20], in which the nacelle had a cylindrical panel that could swing below the inlet during ground

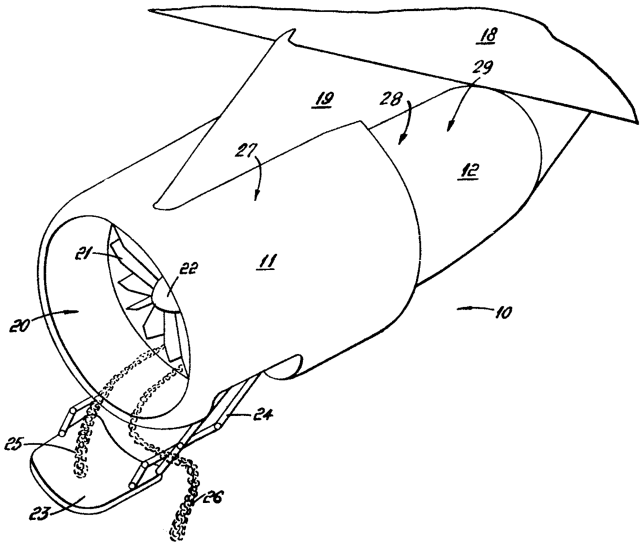

Fig. 13 Cox and William [20] system for inlet-vortex attachment.

operation, thus providing an alternate surface for the vortex to attach, instead than on the ground, where it could suck debris. Figure 13 depicts such system. Testing showed that this assembly was not effective: despite the panel being placed above the usual vortex location, the vortex tended to slip around the panel and still attach to the ground.

Smith [21] designed a system similar to Klein's [2] (Fig. 14), but tried to take into account the movement of the inlet vortex relative to the engine inlet. Smith's [21] system created a wide sheet of air beneath the inlet, impinging the ground away from the inlet centerline, minimizing the dislodgment of debris that could fly into the air and get ingested by the inlet. Smith proposed to place a tube beneath the engine inlet, protruding forward, which would exhaust bleed air through two rows of holes, taking about 0.25% of engine flow and creating a protection curtain, preventing an inlet vortex from building up.

Another invention, in a similar fashion, was proposed by Bigelis et al. [22]; however, it attacked the inlet-vortex problem in a different way. Its principle of operation was based on creating an artificial headwind that would entrain flow beneath the engine "in a direction which prevents the necessary conditions for the origin of a vortex stagnation point," essentially creating an artificial headwind.

More recent studies performed by Funk et al. [23] to assess the effectivity of blowing unsteady jets showed that inlet vortices can be reduced or eliminated with flows in the order of 0.5% of the total engine air flow. However, because the inlet vortex is a transient phenomenon, the stagnation point is always moving, therefore it is difficult to estimate a target point for the jets.

Shmilovich et al. [24] developed another system, trying to take into consideration the inherent problem of sporadic vortex motion by using a movable nozzle injecting fluid (preferably engine bleed air) in the direction of the vortex. They stated that their invention addressed other inventions' shortfalls by considering the fundamental problem of unsteady characteristics of realistic inlet-vortex flows, keeping the invention simple by minimizing the number of moving parts, and eliminating foreign object damage (FOD) due to the active system itself by preventing ground impingement of the control jet. Figure 15 shows under the nacelle the active vortex control system of Shmilovich et al. [24].

III. Vortex Clear-Up Speed

Despite all the inventions described in the previous section, it has not been found, so far, any feasible and economical system that would easily reduce the strength or destroy the inlet vortices that exist during engine high power operation on the ground. The solution usually employed (one of its first proponents being Glenny and Pyestock [4] in 1970) is to minimize the contact of engine inlet stream tube with the ground, avoiding the conditions for the vortices to exist. This means optimizing the inlet stream-tube area, given by

$$A_0 = \frac{W_e}{\rho_0 U_0} \tag{3}$$

where ρ_0 is the ambient air density; W_e is the engine inlet mass flow rate, which is a function of engine thrust; and U_0 is the freestream speed, which depends both on the ambient wind and aircraft speeds. Upon analyzing these parameters, the only ones that the aircraft pilot

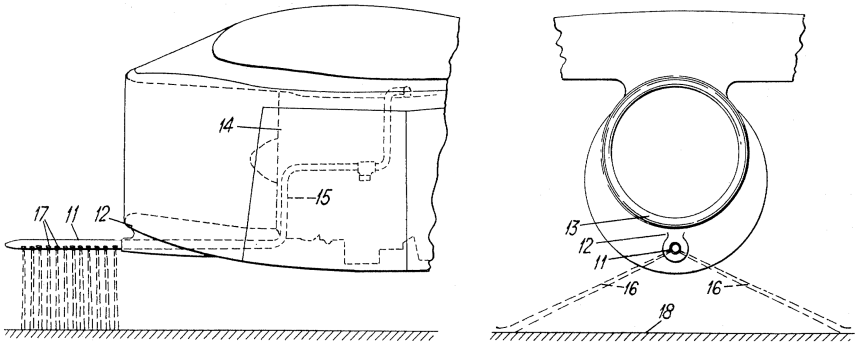

Fig. 14 Smith [21] system where a sheet of air shields the inlet from the vortex, side and forward view, respectively.

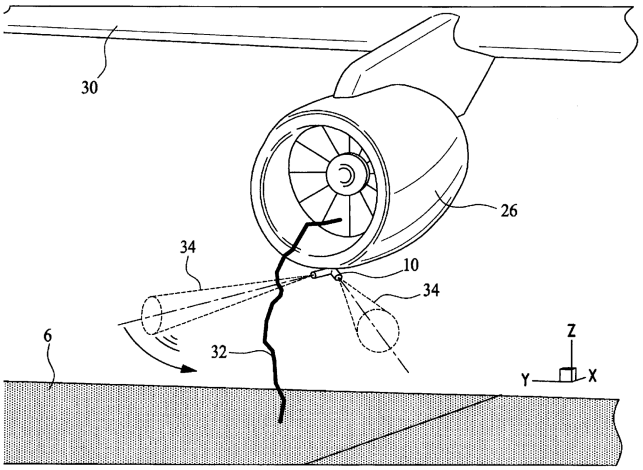

Fig. 15 Active vortex control system installed under the nacelle [24].

has control over (and therefore, can act on to reduce the possibility of vortex formation) are the engine thrust (or mass flow) and the aircraft speed.

Another aspect involved is the engine distance to the ground, which, ideally, shall be as high as possible, allowing space for the greatest possible freestream-tube area A_0. Yet, a large distance between the engine and the ground can increase the landing gear size, allow the engine exhaust jet to interfere with the wing airflow and affect the engine thrust line, among other factors [25]. Therefore, a compromise between all variables must be sought.

For a given engine installation (i.e., for a given engine distance to the ground) and engine thrust, the smallest aircraft speed U_0, at which there is no vortex attached to the ground, is the vortex clear-up speed. The optimal takeoff procedure is to operate the engine at an engine thrust, which varies with aircraft speed and would keep the stream tube close to the ground, but never touch it. As the aircraft accelerates, the thrust is increased in such a way that the stream-tube area is kept constant. The reader shall be aware, however, that when the aircraft is static ($U_0 = 0$) the stream tube has infinite area ($A_0 = \infty$) and there is always a vortex, unless the thrust is zero ($W_e = 0$) when the engine is off.

To illustrate the rationale for the vortex clear-out speed, Fig. 16 shows an engine inlet subject to different headwind condition. In Fig. 16a, there is no wind and the stagnation point is below and forward of the inlet, whereas Fig. 16b shows the inlet with moderate headwind (or moderate aircraft speed). The stagnation point has moved aft and the inlet vortex is longer and weaker; also a stagnation line has formed around the inlet. In Fig. 16c, the wind intensity is stronger and the inlet is above the vortex clear-up speed; the stagnation point has left the ground and there is no vortex present, while the stagnation line on the nacelle has moved toward the inlet.

Many different studies were performed to determine the vortex clear-up speed. They relate engine inlet mass flow ratio with the engine distance to the ground, normally in a parametric form, as the ratio of the distance from the engine axis to the ground H and the fan diameter D_i. Some authors also use highlight diameter D_h and distance from the lip to the ground Z. Figure 17 depicts the different parameters that can be used.

IV. Inlet-Vortex Analysis

Most of the analysis that will be presented here will be performed using the DLR-F6 nacelle [26], a wind-tunnel long-duct nacelle-scaled model from the wing-body-pylon-nacelle configuration used in the AIAA Drag Prediction Workshops. Because this nacelle geometry is open to the general public it can be used in the future to compare results from different authors. The original nacelle is a hollow through-flow nacelle, which does not contain an engine. To use this nacelle model in an actual crosswind CFD simulation, the internal geometry was modified to better represent a real engine, incorporating outlet and inlet boundaries, but no effort was made to

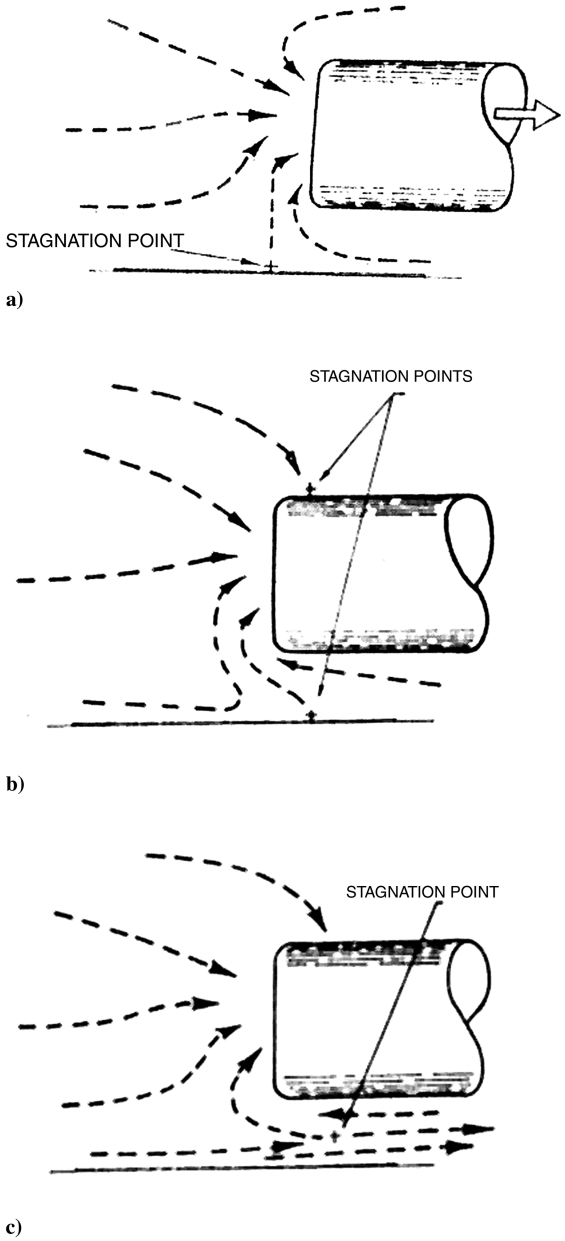

Fig. 16 Stagnation points at different headwind conditions: a) no head wind, b) moderate headwind, and c) strong headwind [10].

add a spinner at the fan plane. Typical dimensions for the DLR-F6 wind-tunnel model nacelle are given on Table 1, together with design parameters.

There are two major inlet design parameters that impact the smoothness of the flow that will reach the engine: the inlet-diffuser ratio and the inlet-contraction ratio. The inlet-diffusion ratio is the ratio between the fan and the inlet throat areas and it influences the air-flow speed on the fan blades. The inlet-contraction ratio is defined as the ratio between the inlet highlight and the inlet throat areas and regulates the flexibility of the inlet to ingest flows that are not aligned with the inlet plane, for example, high angle of attack and crosswind

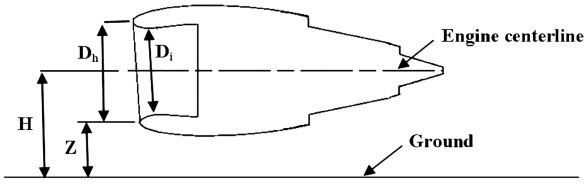

Fig. 17 Nacelle ground clearance parameters.

Table 1 DLR-F6 nacelle dimensions and design parameters

Design parameter	Symbol	Dimension, mm
Length	L	180.0
Highlight diameter	D_h	55.1
Inlet throat diameter	D_i	49.4
Fan diameter	D_f	54.8
Max diameter	D_m	76.2
Exhaust diameter	D_{ex}	50.0
Diffusion ratio	DR	1.10
Contraction ratio	CR	1.24

conditions. The values of the DLR-F6 nacelle inlet-diffusion and contraction ratios are also shown on Table 1.

To assess the nacelle behavior during crosswind operation, it was chosen, as typical condition, sea level, aircraft static, international standard atmosphere day, and a 90° crosswind with wind intensities between 5 and 30 kt. The nacelle was positioned at a distance from the engine centerline to the ground equal to the highlight diameter. The computational domain was hemispherical, with a diameter 50 times the nacelle maximum external diameter.

The CFD analysis were performed using CFD++ [27], a commercial CFD software based on a finite volume formulation, which can deal with arbitrary mesh types. The Reynolds-averaged Navier–Stokes (RANS) three-dimensional equations are solved for the compressible flow using implicit, second-order interpolation, centroidal based polynomials, and preconditioned relaxation. The turbulence model used was realizable k-ε.

At the fan-face boundary either a static pressure or a mass flow rate boundary conditions were used. The mass flow rate imposed was typical of an engine at the same condition, in this case 0.34 kg/s. The domain initial conditions were identical to the far-field boundary conditions, at which a characteristic based velocity inflow/outflow was prescribed, imposing wind speed, temperature, turbulent intensity, and turbulent length.

One of the earlier problems that were faced, after running a CFD analysis with a ground vortex present, was to determine the best way to visualize it. An extensive analysis of current vortex visualization methods was performed [28] to determine the best method or tool. The best way found was the vortex core tool available in the Ensight visualization software [29], which showed the best vortex characterization (Fig. 18), without much noise or interference with other surfaces. However, it still fails to predict the curved vortex core segments, therefore not capturing the ground vortex well on the region where it is turning more steeply into the engine. A turnaround to this problem is to release particle traces from the vortex core, which will approximately show the vortex path. Other problem with this method is that it requires operations to be performed within the mesh grid, which is difficult to implement on a commercial postprocessing code, if the code does not include this feature originally.

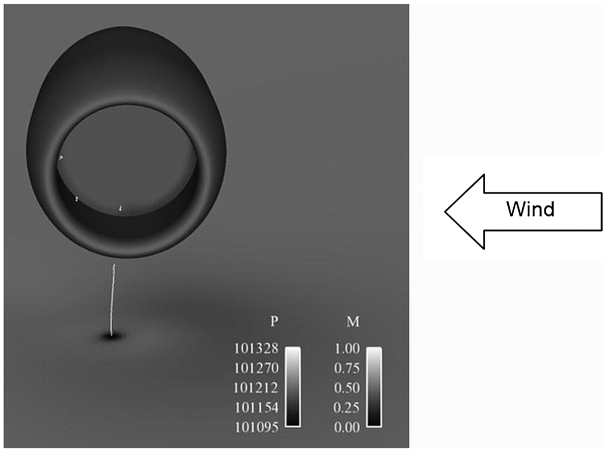

Fig. 18 Mach number isocontours on the nacelle and fan surfaces, vortex cores, and isocontours of static pressure on the ground at 5 kt crosswind, fan static pressure equal to 90,000 Pa, $H/Di = 1.13$; inviscid analysis.

A. Influence of Viscosity and Separation

Many industrial applications of CFD are today still limited by computational resources and cannot be simulated in its full complexity; the simulation of the inlet-vortex phenomenon is one of these cases. It is thus necessary to use turbulence models and to restrict the analysis to steady state. An initial set of numerical tests was performed with the nacelle, starting with smaller meshes and inviscid flow, before proceeding to the viscous cases with larger meshes. These simplifications were also tested to compare the results with the ones obtained by other authors, who employed simpler tools.

For the inviscid simulations, in which the Euler equations were solved, the isolated nacelle mesh contained 3 million tetrahedral elements. For the viscous analyses, hybrid grids containing nearly 5 million elements were used. The parameter $y+$, which is important in evaluating the ability of the grid to capture near-wall effects, was less than 1 in all viscous cases.

Results for a 5 kt crosswind are depicted in Fig. 18, which displays the vortex core, isocontours of Mach number on the nacelle and fan surfaces, and static pressure isocontours on the ground. It is possible to see the inlet vortex attached to the ground surface, where it creates a low-pressure region. The Mach number on the inlet lip is close to sonic.

The same inviscid case was run at 20 kt. The results showed that there was flow separation at the inlet lip and, also, that the inlet vortex was blown away by the wind, being detached from the ground (Figs. 19a). This vortex detachment from the ground was unexpected, given that actual aircraft engines at equivalent operating conditions show very clear inlet vortices. Therefore, this case was then compared to a viscous case, with a modified mesh, where prism layers were added to all wall surfaces of the original tetrahedral mesh. These results can be seen in Figs. 19a and 19b and show a remarkable difference on the ground vortex behavior, which in the viscous case is now kept attached to the ground, being more consistent with the actual case.

Another difference between the inviscid and viscous results was the different shape of the separated flow region, which is elliptical in the inviscid case and has a crescent shape in the viscous case. The elliptical separation region of the inviscid case seems more coherent with the shape of the expected separation bubble. However, in the viscous case, where the inlet separation and the inlet vortex coexist, they interact over each other and the inlet vortex locally pulls the separation region toward itself, in the edge of the crescent shape. Therefore, the difference between the separated regions of Fig. 19 is because one case has an inlet vortex and the other one does not (not because of the viscosity).

Because of the detached inlet vortex on the inviscid case, it is clear that the viscosity plays an important role on the inlet-vortex phenomenon and, contrary to Viguier [12], the fluid viscosity cannot be disregarded when evaluating the inlet vortices. Results support Nakayama and Jones's [13] conclusions that the inviscid analysis produces a lower vortex clearance speed. It is also important to stress that even though the analysis was inviscid, numerical codes always present some sort of numerical diffusion, which may lead to the production of vorticity in the solution. As a consequence, the inviscid solution inlet vortex may have little resemblance with an ideal inviscid flow vortex. However, because of the initial differences between the viscous and inviscid solutions, an inviscid analysis methodology was discarded and the representativeness of the CFD inviscid solution was not investigated further.

The engine inlets used on real applications usually operate without flow separation because it affects engine operability and fan blade aerodynamics, therefore the DLR-F6 nacelle was modified to eliminate this inlet-flow separation. This was achieved by changing the inlet lip lofting and the contraction ratio. The nacelle lip cross section, originally circular, was turned into elliptical, with the ratio between the minor and major axis of the ellipse equal to 2.5, while the contraction ratio was increased from 1.24 to 1.32. This nacelle was

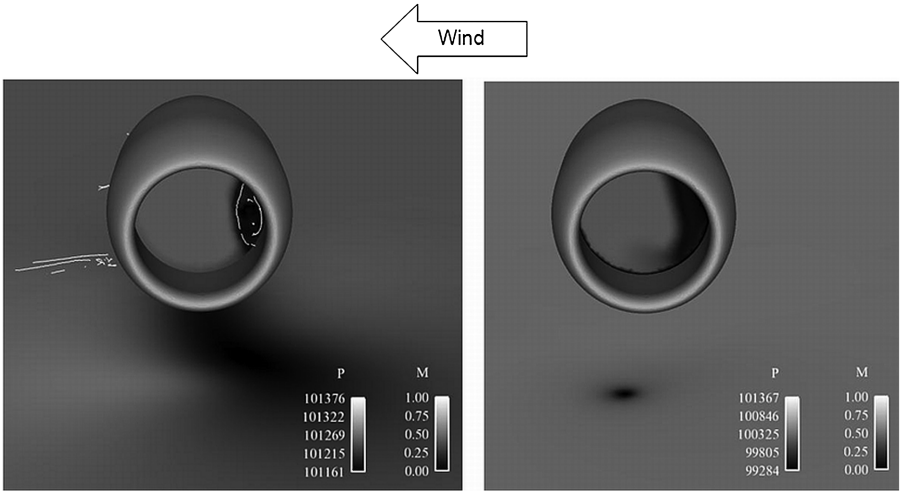

a) b)

Fig. 19 Mach number isocontours on the fan surface and static pressure isocontours on the ground at 20 kt crosswind. Fan static pressure equal to 90,000 Pa, $H/Di = 1.13$: a) Euler and b) Navier–Stokes analyses. The inviscid case also shows vortex cores.

named DLR-F6 MOD2. Results for this MOD2 nacelle, under a 20 kt crosswind, can be seen on Fig. 20a. It is interesting to notice that the vortex intensity became more intense, compared to the separated nacelles of Figs. 19a and 19b. This vortex intensity increase was due to the boundary condition used in the fan plane, at which a constant static pressure was assigned. If a constant static pressure outlet boundary condition is imposed and there is inlet separation, the intake recovery decreases and therefore the mass flow into the engine also decreases, which then lowers the vortex intensity. If the boundary condition is set to maintain the same mass flow ratio, the vortex core pressure stays at approximately the same level, which was occurred when the CFD case was run again with an imposed mass flow boundary condition (see Fig. 20b). These results show that care shall be taken when designing experimental setups; some experiments in the literature involved the use of simple pipes with suction on one side to represent a nacelle. If these pipes had flow separation at their inlets when being tested in a crossflow, the experiment would have produced inlet vortices of lower intensity, whereas a well designed pipe inlet would have produced much clearer vortices. It is also important to point out that the real situation in an engine, with a separated inlet, would be a more complex case to determine, because the separation reduces inlet efficiency and affects engine performance. In an engine with a separated inlet, the engine control would attempt to maintain the rotors' speeds to compensate the losses in the inlet, increasing the fuel feed, but may be subject to some limitation (turbine temperature, for instance). Additionally, the separation affects the fan blade aerodynamics, leading to drop in fan efficiency, which may allow the rotors to keep their speeds more easily, needing less fuel flow, but also producing less thrust and taking less inlet mass flow, therefore producing a lower intensity vortex.

B. Pressures on the Ground

After a proper nacelle inlet configuration was found (the DLR F6 MOD2 nacelle), which would not bring about flow separation at high mass flow ratios and under strong crosswinds, the computational mesh was refined further in the inlet vortex region to ensure proper capture of the phenomenon. The updated mesh can be seen in Fig. 21, which shows viscous CFD results of static pressure on the ground for the high thrust static case (fan mass flow rate of 0.34 kg/s), allowing a comparison between the size of the mesh and the vortex size.

To understand the inlet-vortex behavior as a function of the mass flow ratio, different cases were analyzed, with a constant crosswind intensity of 20 kt. Figure 22 shows a plot of minimum pressure

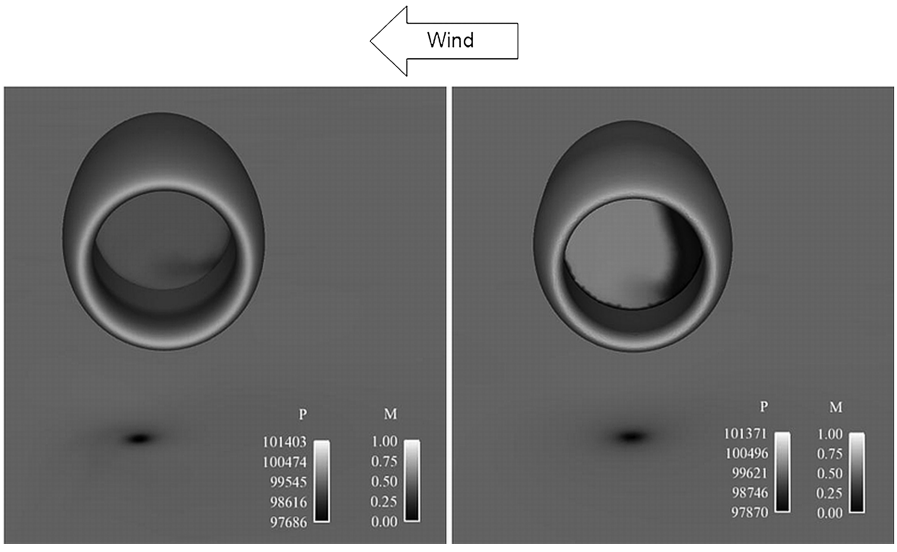

a) b)

Fig. 20 Mach number isocontours on the MOD2 fan surface and static pressure isocontours on the ground at 20 kt crosswind with the following boundary conditions: a) static pressure (90,000 Pa) and b) mass flow rate (0.34 kg/s).

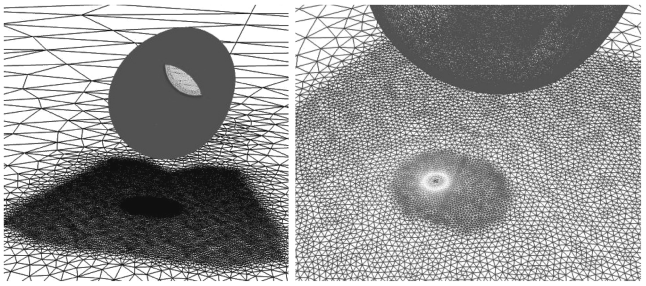

Fig. 21 View of the nacelle and the ground mesh and zoom on the ground vortex location with pressure contours for a high-thrust static case.

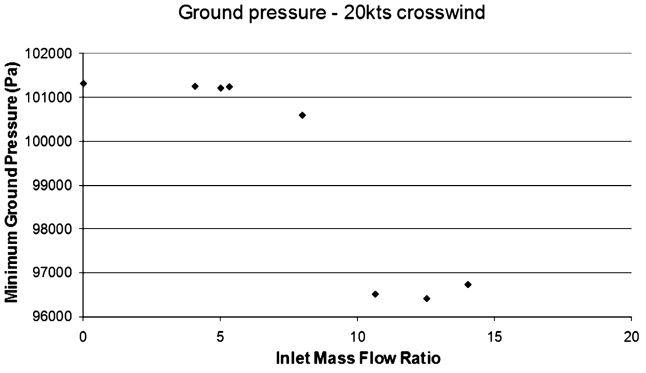

Fig. 22 Minimum ground pressure induced by the vortex as a function of inlet mass flow ratio.

induced on the ground by the inlet vortex as a function of the inlet mass flow ratio. The results show that at low mass flow ratios, the minimum ground pressure remains approximately equal to the ambient pressure. Then, as the mass flow ratio goes beyond 6, the pressure decreases suddenly, until reaching a mass flow ratio of 10, when the minimum pressure reaches another plateau. The inlet-vortex flow seems to be composed of three different flow regimes: 1) one at ambient pressure, without signs of a vortex; 2) a transient regime, where suction at the ground increases suddenly; and 3) a strong vortex regime, where the ground pressure is approximately constant.

According to the literature review, a condition necessary for the vortex to exist is that the inlet stream tube encompasses the ground [8,10,13], implying that the distance from the engine centerline to the ground H, shall be less than the radius of the inlet stream tube. To evaluate how the inlet stream tube contact with the ground affects the inlet vortex, it was defined a parameter called the stream-tube diameter ratio (SDR). The SDR, as shown in Fig. 23, is the ratio between the ideal stream-tube diameter D_0 and the diameter of an imaginary cylinder of radius equal to the distance from the engine

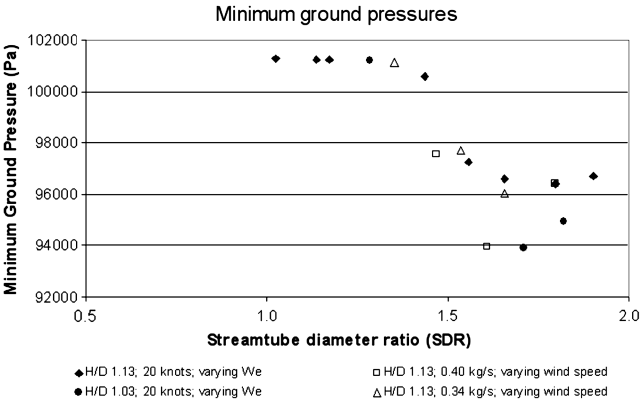

Fig. 24 Minimum ground pressure induced by the vortex as a function of stream-tube diameter ratio for varying engine mass flow rates, inlet to ground distances, and crosswind intensities.

axis to the ground H. The ideal stream tube is the axisymmetrical stream tube of an isolated nacelle undisturbed by the ground. This definition implies that when the SDR is greater than one the inlet stream tube encompasses the ground and an inlet vortex may exist.

The presence of the ground will obstruct part of the ideal stream tube, which will grow in the other directions to keep the same cross-sectional area. This stream tube, called the corrected stream tube (Fig. 23), has a clipped circular cross section and interferes with the ground over a distance L_i called the interference length.

Additional cases were run to evaluate how the ground pressures varied not only as a function of the SDR, but also as a function of the inlet mass flow rate, the crosswind intensity, and the distance from the inlet to the ground. Figure 24 shows the results of minimum ground pressure as a function of the SDR for the following cases: 1) 20 kt crosswind, inlet height ratio of 1.03, and different engine mass flow rates; 2) 20 kt crosswind, height ratio of 1.13, and different engine mass flow rates; 3) inlet mass rate of 0.40 kg/s, height ratio of 1.13, and different crosswind intensities; and 4) inlet mass rate of 0.34 kg/s, height ratio of 1.13, and different crosswind intensities. It can be seen that the sudden drop in the minimum ground pressure is occurring at approximately the same SDR of 1.4 for all cases, achieving a minimum pressure at an SDR of approximately 1.6. This similar behavior among the different cases shows that the SDR seems to be a good parameter to evaluate the inlet-vortex existence and its strength.

On the other hand, the plot of Fig. 24 also shows that the sudden drop in minimum pressure is not occurring at a SDR of one, when the ideal stream tube would start getting in contact with the ground. This may be because the actual inlet stream-tube cross section is not exactly circular, meaning that it is not yet getting in contact with the ground when SDR is one. Another reason may be that the stream tube must have a minimum area interfering with the ground before the inlet vortex can gain strength.

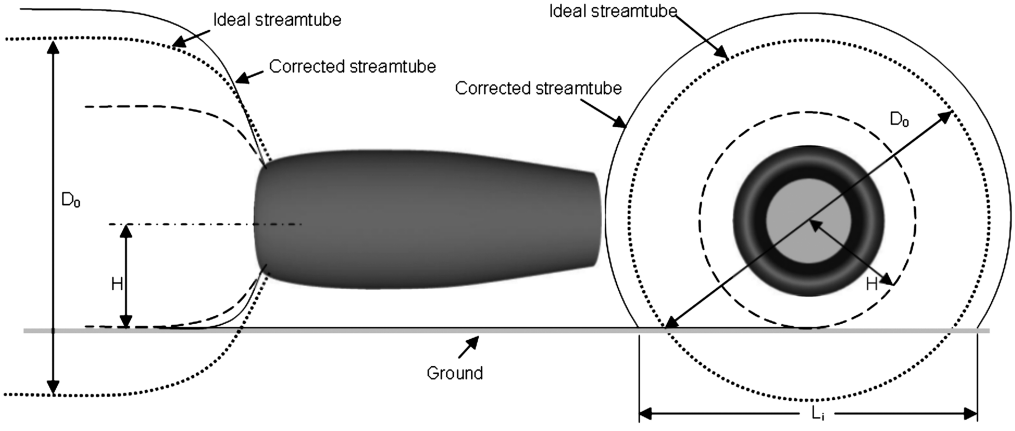

Fig. 23 Nacelle inlet stream tube definitions, side view, and front view, respectively.

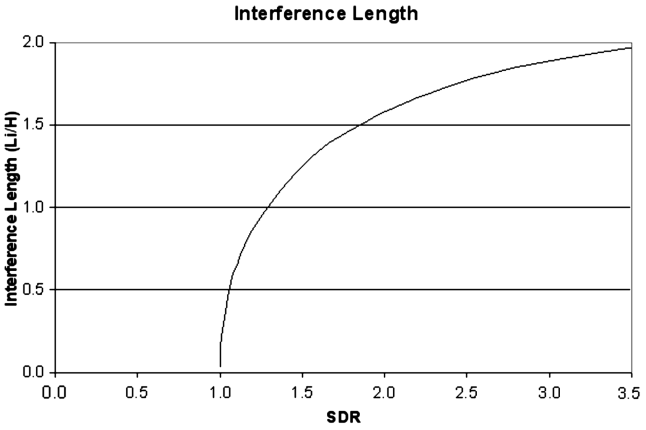

Fig. 25 Stream-tube interference length as a function of the SDR.

Another aspect of Fig. 24 that is worth mentioning is that the strong vortex regime, once achieved at SDR 1.6, does not always keep a constant ground pressure. In some cases, the minimum ground pressure, after reaching an absolute minimum around SDR 1.6, increased slowly.

The sudden drop in the minimum ground pressure, between SDR 1.4 and 1.6, seems to be linked to the interference length. When the engine distance to the ground varies, the interference length will also vary to maintain the area of the corrected stream-tube cross-sectional constant, according to the following relationship:

$$A_0 = \frac{D_0^2}{4}\left\{\pi - \arctan\left(\frac{H}{L_i}\right) + \frac{1}{2}\,\text{sen}\left[\arctan\left(\frac{H}{L_i}\right)\right]\right\} \qquad (4)$$

This equation was solved to find the interference length as a function of the SDR. These results are shown in Fig. 25, where the interference length is adimensionalized by the inlet distance to the ground. It is interesting to notice the exponential growth of the interference length once the stream tube has got in contact with the ground. Having a greater interference length means that the inlet stream tube is able to collect more vorticity from the ground, which intensifies the inlet-vortex strength.

To use the CFD results to evaluate the relationship between the inlet stream tube and the inlet vortex, it is necessary to estimate the actual stream-tube cross section. The cross section of an inlet stream tube aligned with the external flow can be easily estimated; however, when the inlet flow is highly misaligned and is interacting with the ground (and its boundary layer), the stream tube is harder to define. One possible way to estimate the stream-tube limits is to release streamlines from the edge of the fan-face boundary condition and check where they depart from. Because these streamlines define the boundaries of the inlet flow, they shall also define the limits of the inlet stream tube.

Figure 26 shows the streamlines that reach the fan-face edges, together with pressure contours on the ground, for stream-tube diameter ratios of 1.1, 1.2, 1.4, and 1.8, respectively. In the case with SDR equal to 1.1 (Fig. 26a), a couple of low-intensity trailing vortices can be noticed downstream of the nacelle. The streamlines in the bottom of the nacelle are more concentrated than those in the top,

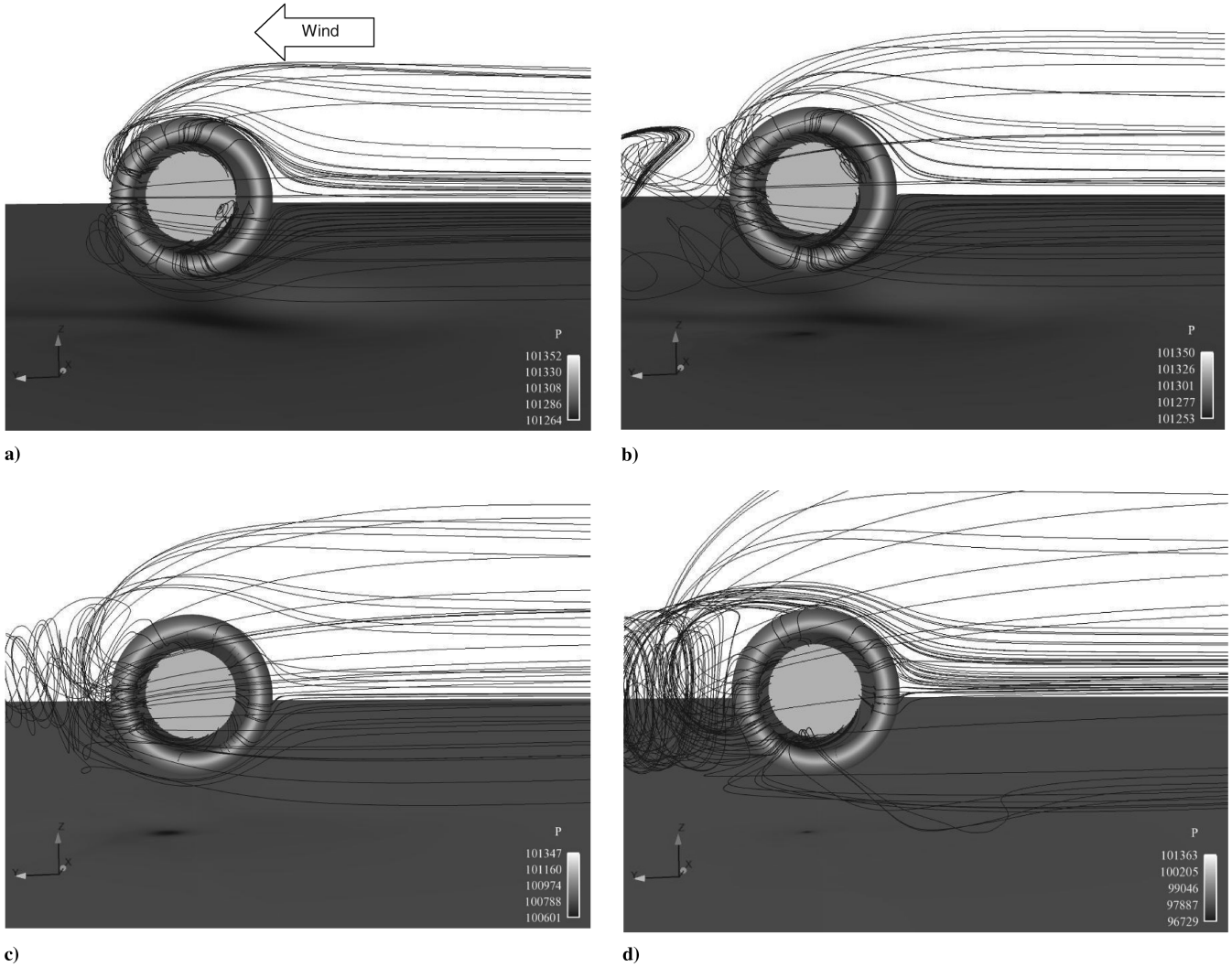

Fig. 26 Streamlines reaching the edge of the fan face, ground colored by pressure contours, with stream-tube diameter ratios of 1.0, 1.2, 1.4, and 1.8, respectively. Wind blowing from the right-hand side.

showing that the inlet stream tube is shifted slightly upward. When the flow into the nacelle is increased and the stream-tube diameter ratio becomes 1.2 (Fig. 26b), the interference of the stream tube with the ground becomes larger and the trailing vortices increase their lengths, becoming, in this case, asymmetrical, with the top trailing vortex being longer than the bottom one. Also, a low-pressure spot now appears on the ground, yet with an intensity of just a few pascals lower than ambient. It is also worth mentioning that on this case, if particles are released from the low-pressure region on the ground, a vortex becomes visible. Thus it seems that three vortices are present: two trailing vortices and a inlet vortex. However, these results come from a steady-state RANS simulation and they may be an intermediate solution, in which the inlet vortex and the lower-trailing vortex alternately exist in an unstable manner. In the case with SDR equal to 1.4, shown in Fig. 26c, where the mass flow ratio was increased further, the bottom trailing vortex disappeared from the results, but the pressure on the ground remains low. Then, with a higher flow ratio (SDR 1.8), the inlet vortex becomes strong and the minimum pressure on the ground becomes much lower than in the previous cases.

Nevertheless, as it can be seen in Figs. 26b–26d, the streamlines released from the edge of the boundary condition failed to encompass the vortex on the ground, even if the number of streamlines was increased to 500, showing that this is not a good method to identify the boundaries of the stream tube. Only when particles are released from the whole fan plane the whole stream tube can be visualized.

A comparison between the flow with a strong vortex and the flow with a weak vortex brings additional insights into the inlet-vortex phenomenon. An approximate visualization of the stream tube that reaches the nacelle for the SDR 1.2 and 1.8 cases is presented in Fig. 27, which shows a leeward side view of the nacelle, with the streamlines that are captured by the inlet, now being released from the whole boundary condition. Upon comparing both cases, it can be seen the stream tube in the case with SDR 1.2 has an approximately elliptical cross section, whereas the higher SDR case has a distorted cross section, interacting more intensively with the ground. Figure 27 also shows that the interface between the stream tube and the ground is different between the two cases: whereas at the SDR 1.2 case, the stream tube reaches the ground at sharper angle; at the SDR 1.8 case, the stream tube reaches the ground more smoothly and spreads more widely on the ground, interacting with the ground over a greater interference length.

To verify the source of the vorticity being ingested by the inlet, for the stream-tube ratios of 1.2 and 1.8, an isosurface of vorticity with intensity 3000 s^{-1} (see Fig. 28) was created. The SDR equal 1.8, which has a strong inlet vortex, is sucking a large volume of vorticity from the ground boundary layer and it is this ground vorticity that intensifies the inlet vortex. This shows that for a strong inlet vortex to exist, the inlet stream tube shall be not only in contact with the ground, but this contact shall be over a wide area, allowing the inlet to ingest more ground vorticity, which is then intensified.

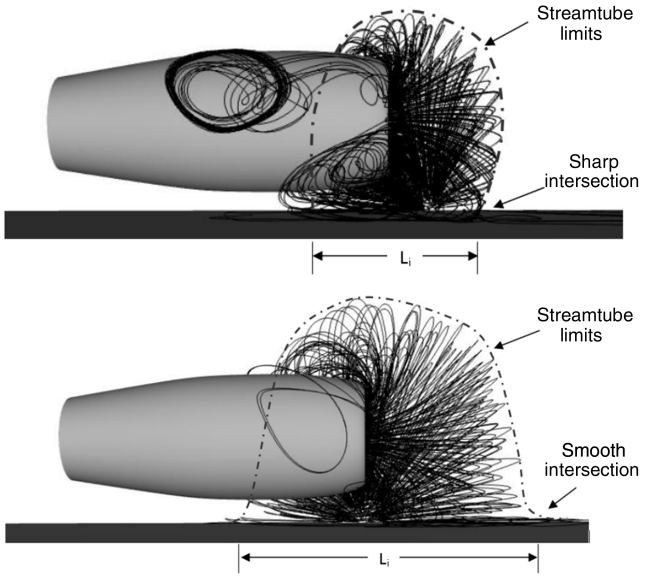

Fig. 27 Leeward side view of the nacelle with streamlines that enter the inlet for a SDR of 1.2 and 1.8, respectively.

C. Trailing Vortex

A trailing vortex usually coexists with the inlet vortex when the inlet is operating at high power in a crosswind. An initial CFD analysis, with another nacelle and no ground, showed that there was a pressure recovery loss inside the inlet, on the leeward side. This pressure loss was due to two small vortices located on the fan-face leeward diagonal. Figure 29 shows contours of longitudinal vorticity at the fan face, showing traces of these two contrarotating vortices. These vortices extend downstream of the nacelle, initially seeming to be coherent with the figures produced by Liu et al. [8] as previously showing in Fig. 7.

However, Liu et al.'s [8] vortices were not ingested by the inlet once the capture area does not encompass them. When a more detailed look is taken of the CFD results (Fig. 30), plotting the streamlines that reach the two counter-rotating vortices at the fan-face boundary, it can be seen that the vortices are actually ingested by the engine and do not flow downstream of the inlet. In fact, the trailing vortices are composed of vorticity generated on the nacelle external wall, which rolls into a wake similar to the that of a cylinder in a crossflow. This wake is initially blown downstream by the crosswind; however, it loses speed because of the engine suction, flows upstream, and is finally drawn back and ingested by the inlet.

If one were to adapt the figure of Liu et al. [8] to the correct representation, it would look like the one on Fig. 31.

The vortex behavior can be better understood taking a look on an isolated, finite cylinder under a crossflow, which was analyzed on an earlier stage of this work as an initial evaluation of the numerical methods and the numerical mesh. The plot of vortex cores [29] of a 20 kt crossflow over a cylinder with dimensions similar to that of the DLR F6 nacelle is shown on Fig. 32.

There are four pairs of vortices on the isolated cylinder: one on each side wall because of the separation of the incoming flow on the sharp edge and two on the back because of the roll of the vorticity on the cylinder wall. The vorticity is washed away by the flow coming to the cylinder sides, becoming longitudinal vortices. According to classical vortex theory, these longitudinal vortices would extend to infinity, where they connect with the starting vortex.

When there is suction on the side of the cylinder (as the case of the nacelle with an engine operating), the sidewall vortex is sucked into the engine and disappears. The longitudinal vortices stay, but the connection between the upper and lower vortices is sucked into the engine. The vorticity generated by the cylinder walls rolls up in two vortices that are initially blown by the crosswind until they are captured by the flow coming back into the engine. One possible explanation for Liu et al.'s [8] trailing vortices behind the inlet and outside the capture area is that those vortices were not inlet vortices but another set of vortices generated on the back of the pipe used on

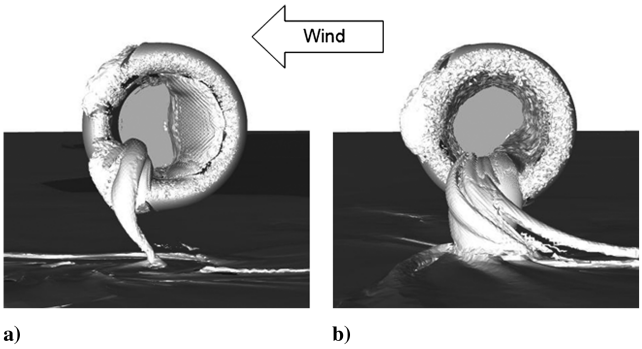

Fig. 28 Isosurface of vorticity with intensity 3000 s^{-1}, for the cases with a) SDR = 1.2 and b) SDR = 1.8.

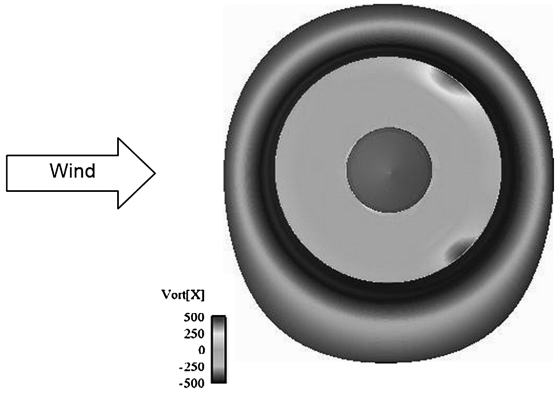

Fig. 29 Contours, on the fan plane, of vorticity in the engine axis direction, with 20 kt crosswind.

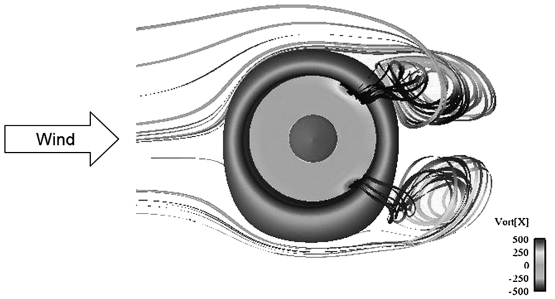

Fig. 30 Flow path of the contrarotating vortices on the leeward side on the inlet. The fan plane is colored by vorticity in the engine axis direction, whereas the streamline by vorticity magnitude.

their experiment. These vortices would also tend to detach but would not be sucked into the engine, rather following the flow downstream.

The trailing vortex with the ground present exhibits a behavior similar to the isolated nacelle; but instead of two vortices, only one exists, as can be seen in Fig. 33. The figure shows a plan view of the nacelle and ground, with streamlines released from the trailing-vortex core. The ground is colored with pressure isocontours and the effect of inlet vortex can be seen on the low pressure region in front of the nacelle. The streamlines are colored by speed intensity in the wind direction. The single trailing vortex is being formed again by vorticity on the back of the nacelle, which flows downstream in a cylinder wake fashion, but eventually loses speed and gets captured back to the inlet in a more concentrated vortex.

D. Comparison of Vortex Clear-Up Speeds

As already discussed, a condition necessary for an inlet vortex to exist is that the engine inlet stream tube be in contact with the ground. As a consequence, the vortex clear-up speed is a function of the free area between the engine and the ground, which means that it shall vary with the square of the engine inlet distance to the ground. Taking the vortex clear-up data that Nakayama and Jones [13] collected and finding the best fit with a second-order polynomial function, it is proposed that the vortex clear-up speed U_0 follows:

$$\text{MFR} = \frac{U_i}{U_0} = 7.64\left(\frac{H}{D_i}\right)^2 - 0.15 \tag{5}$$

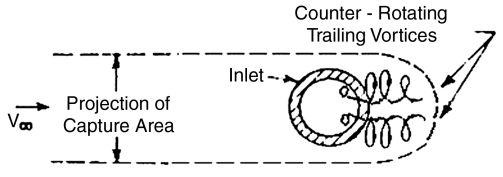

Fig. 31 Correct representation of the trailing vortices.

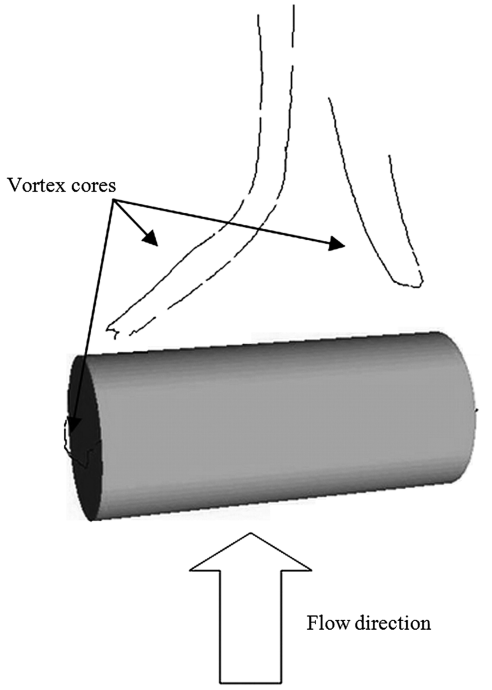

Fig. 32 Vortex cores on an isolated finite cylinder on a crossflow.

This equation is plotted in Fig. 34, together with Nakayama and Jones's [13] original linear equation and the experimental data from the literature, showing very small differences with regard to the results of the original equation, but being more correct from the physical standpoint.

The proposed equation was then compared to Nakayama and Jones [13] and the present CFD results, but splitting the CFD results into three groups: the weak and strong vortex regimes and the case where there was no vortex present. The comparison between the vortex clear-up speed equations and the CFD results for the strong vortex showed good agreement. The weak vortices seem not to be covered by the correlations, perhaps because of the difficulty to capture them experimentally.

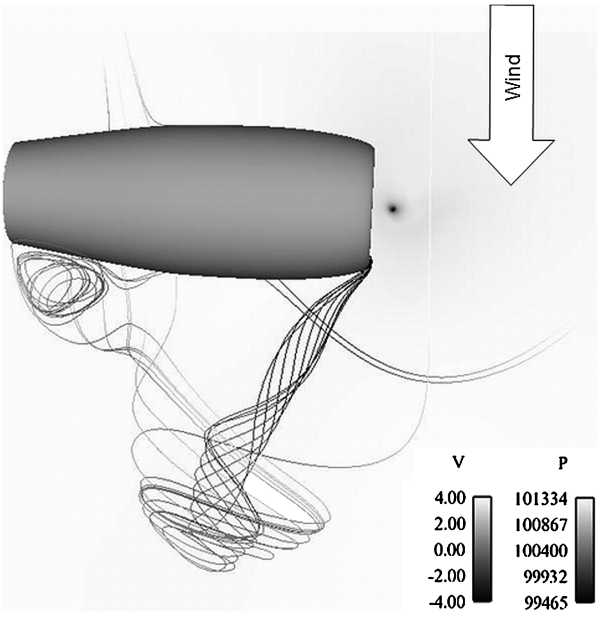

Fig. 33 Plan view of the nacelle, showing the streamlines on the trailing vortex colored by streamwise velocity, ground colored by pressure isocontours.

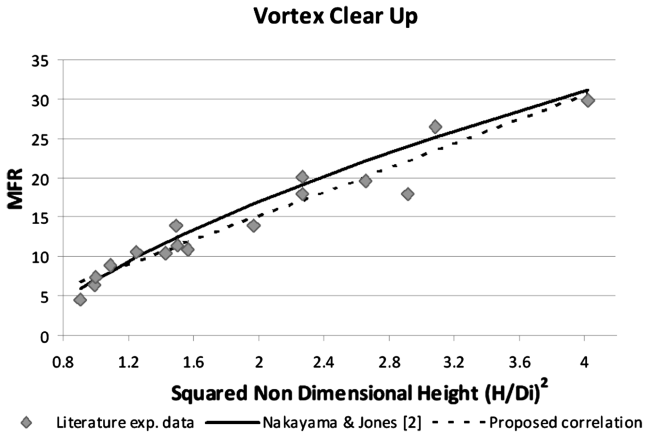

Fig. 34 Comparison between literature experimental data Nakayama and Jones [13] and the proposed equation.

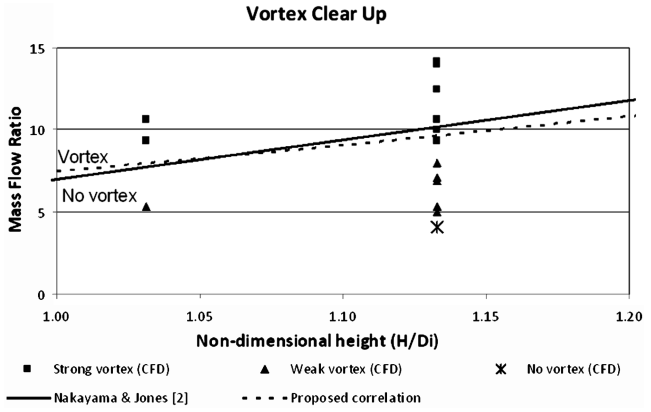

Fig. 35 Comparison between proposed vortex formation correlation from Nakayama and Jones [13] and the CFD data.

V. Conclusions

The comparison of inlet-vortex results between viscous and inviscid calculations showed differences, with the vortex in the inviscid cases, detaching from the ground at a lower crosswind speed than the viscous case. Additionally, the detachment of the inlet vortex from the ground, in the inviscid analysis, caused the inlet separation pattern to be different than the viscous case. Therefore, even though, in general, vortical flows are considered to be inviscid, the interaction of the inlet vortex with the ground shear layer has a viscous effect that needs to be taken into account.

Inlet separation was shown to influence the inlet-vortex strength, depending on the boundary condition used to represent the engine fan, with a separated inlet vortex being less strong than an attached inlet one. Consequently, it is possible for a nacelle inlet with flow separation at high crosswinds to be less susceptible to foreign-object ingestion than the same nacelle at lower crosswinds with an attached inlet flow.

The existence of the inlet vortex is conditioned to the interference between the inlet stream tube and the ground surface. A parameter called the SDR was defined to evaluate the level of existing interference and therefore estimate the strength of the inlet vortex. This parameter showed that three inlet-vortex regimes existed: a weak vortex regime between SDR 1.1 and 1.4 with minimum ground pressures close to the ambient pressure, a transient regime between 1.4 and 1.6, where the minimum pressure dropped suddenly, and a strong vortex regime at SDR greater than 1.6.

The CFD results also presented good correlation with the ones presented in the literature when a strong vortex was present. The weak vortex has such a low intensity that apparently not even the experiments were able to capture it. This may not be a problem when trying to avoid damage by FOD, but the vortex may be strong enough to suck in small particle of sand, such as the ones present in airports in the Middle East, causing erosion and clogging of combustors and turbine blade cooling passages.

The inlet stream tube in crosswind conditions cannot be captured automatically with postprocessing tools. The stream-tube contours can be estimated by releasing streamlines, but because of the influence of the inlet vortex, these streamlines have to be released over the full inlet boundary condition plane, not only close to its border.

The existence of contrarotating trailing vortices, on nacelles both isolated and near the ground, was shown to be caused by the nacelle wake. It was shown that the trailing vortex does not extend downstream infinitely, but it is held by the inlet flow and sucked back into the engine.

Based on literature experimental data, a new correlation for the vortex clear-up speed was proposed. This formulation is based on the square of the nondimensional height and matches well the experimental data and also being better related to the phenomenon physics than the original linear relationship from Nakayama and Jones [13] and the present CFD results on Fig. 35.

Acknowledgment

The author would like to thank Embraer for the resources and time made available to perform the current studies.

References

[1] "Inlet Total-Pressure-Distortion Considerations for Gas-Turbine Engines," SAE International Rept. AIR-1419, Rev. A., March 1999.

[2] Klein, H. J., U.S. Patent for "Vortex Inhibitor for Aircraft Jet Engines," Douglas Aircraft Co., No. 2,915,262. B64D33/02, filed 1 Dec. 1959.

[3] Rodert, L. A., and Garrett, F. B., "Ingestion of Foreign Objects into Turbine Engines by Vortices," NACA TN-3330, Washington, D.C.,1955.

[4] Glenny, D. E., and Pyestock, N. G. T. E., "Ingestion of Debris into Intakes by Vortex Action," Aeronautical Research Council, Paper 1114, London, 1970, pp. 1–50.

[5] Shin, H. W., Greitzer, E. M., Cheng, W. K., Tan, C. S., and Shippee, C. L., "Circulation Measurements and Vortical Structure in an Inlet-Vortex Flow Field," *Journal of Fluid Mechanics*, Vol. 162, Jan. 1986, pp. 463–87,. doi:10.1017/S0022112086002124

[6] Klein, H. J., "Small Scale Tests on Jet Engine Pebble Aspiration," Douglas Aircraft Co. Rept. SM-14885, Long Beach, CA, 1953.

[7] De Siervi, F., "A Flow Visualization Study of the Inlet Vortex Phenomenon," M.Sc. Dissertation, Massachusetts Inst. of Technology, Cambridge, MA, 1981.

[8] Liu, W., Greitzer, E. M., and Tan, C. S., "Surface Static Pressures in an Inlet Vortex Flow Field," *Journal of Engineering for Gas Turbines and Power*, Vol. 107, No. 2, 1985, pp. 387–94.

[9] Brix, S., Neuwerth, G., and Jacob, D., "The Inlet-Vortex System of Jet Engines Operating Near The Ground," AIAA Paper 2000-3998, June 2000.

[10] Colehour, J. L., and Farquhar, B. W., "Inlet Vortex," *Journal of Aircraft*, Vol. 8, No. 1, 1971, pp. 39–43. doi:10.2514/3.44224

[11] Motycka, D. L., Walter, W. A., and Muller, G. L., "An Analytical and Experimental Study of Inlet Ground Vortices," AIAA Paper 1973-1313, Nov. 1973.

[12] Viguier, H. C., "A Secondary Flow Approach to the Inlet Vortex Flow Field," M.Sc. Dissertation, Massachusetts Inst. of Technology, Cambridge, MA, 1980.

[13] Nakayama, A., and Jones, J. R., "Correlation for Formation of Inlet Vortex," *AIAA Journal*, Vol. 37, No. 4, 1999, pp. 508–10. doi:10.2514/2.743

[14] Tourrette, L., "Navier–Stokes Simulations of Air-Intakes in Crosswind Using Local Preconditioning," AIAA Paper 2002-2739, June 2002.

[15] Secareanu, A., Moroianu, D., Karlsson, A., and Fuchs, L., "Experimental and Numerical Study of Ground Vortex Interaction in an Air-Intake," AIAA Paper 2005-1206, Jan. 2005.

[16] Yadlin, Y., and Shmilovich, A., "Simulation of Vortex Flows for Airplanes in Ground Operations," AIAA Paper 2006-0056, Jan. 2006.

[17] Rehby, L., "Jet Engine Ground Vortex Studies," M.Sc. Dissertation, Cranfield Univ., Cranfield, England, U. K., 2007.

[18] Johns, C. J., "The Aircraft Engine Inlet Vortex Problem," AIAA Paper 2002-5894, Oct. 2002.

[19] Lee, S. T., U.S. Patent for "Engine Inlet Protective Screen Arrangement," No. 3,298,637. F02C7/05, filed 17 Jan. 1967.
[20] Cox, P. O., and William, J., Rolls Royce Engines, U.S. Patent for "Pod for a Gas Turbine Engine," No. 3,474,988. F02C7/05, filed 28 Oct. 1969.
[21] Smith, J. P., Hawker Siddeley Aviation, U.S. Patent for "Protective Air Curtain for Aircraft Engine Inlet," No. 3,527,430. F02C7/05. 8 Aug. 1970.
[22] Bigelis, C. F., Colehour, J. L., Davidson, G. D., Farqhar, B. W., and Helberg, A., The Boeing Co., U.S. Patent "Vortex Preventing Apparatus for Aircraft Jet Engines," No. 3,599,429, filed 2 May 1969.
[23] Funk, R., Parekh, D., Smith, D., and Dorris, J., "Inlet Vortex Alleviation," AIAA Paper 2001-2449, June 2001.
[24] Shmilovich, A., Yadlin, Y., Smith. D. M., and Clark, R. W., The Boeing Company, U.S. Patent for "Active System for Wide Area Suppression of Engine Vortex," No. 6,763,651. F02C7/04, filed 25 Oct. 2002.
[25] Oliveira, G. L., Trapp, L. G., and Puppin-Macedo, A., "Engine-Airframe Integration Methodologies for Regional Jet Aircrafts with Underwing Engines," AIAA Paper 2003-0934, Jan. 2003.
[26] DLR-F6 Geometry, DLR, Cologne, Germany, 2006.
[27] "CFD++ v.7.1.1 User Manual," Metacomp Technologies, Inc., Agoura Hills, CA2007.
[28] Trapp, L. G., Argentieri, H. G., Souza, F. J., and Girardi, R. M., "Wind Effects on Isolated Nacelles Near the Ground," *Proceedings of the 11th Brazilian Congress of Thermal Sciences and Engineering*, Paper CIT06-0740, Brazilian Society of Mechanical Sciences and Engineering, Curitiba, Brazil, 2006.
[29] "Ensight User's Manual for Version 8.0," Computational Engineering International, Inc., Apex, NC, 2005.
[30] Campbell, J. F., and Chambers, J. R., *Patterns in the Sky: Natural Visualization of Aircraft Flow Fields*, NASA Langley Research Center, Hampton, VA, 1994.